Dipole source analysis of auditory brain stem responses evoked by lateralized clicks

Helmut Riedel, Birger Kollmeier
Medizinische Physik, Universität Oldenburg

Abstract

The objective of this paper was to elucidate the relation between psychophysical lateralization and the neural generators of the corresponding auditory evoked potentials. Auditory brain stem responses to binaural click stimuli with different interaural time- and level differences were obtained in 12 subjects by means of multi-channel EEG recording. Data were modeled by equivalent current dipoles representing the generating sources in the brain. A generalized maximum-likelihood method was used to solve the inverse problem, taking into account the noise covariance matrix of the data. The quality of the fit was assessed by computing the goodness-of-fit as the outcome of a χ^2-test. This measure was advantageous compared to the conventionally employed residual variance. At the latency of Jewett wave V, there was a systematic variation of the moment of a rotating dipole with the lateralization of the stimulus. Dipole moment trajectories of stimuli with similar lateralization were similar. A sign reversal of the interaural differences resulted in a mirrored trajectory. Centrally-perceived stimuli corresponded to dipoles with the largest vertical components. With increasing lateralization, the vertical component of the moment decreased, while the horizontal components increased. The similarity of trajectories induced by the same lateralization show that interaural time- and level differences are not processed independently. The present data support the notion that directional information is already extracted and represented at the level of the brain stem.

Keywords: ABR, lateralization, ITD, ILD, dipole source analysis

Zusammenfassung

Das Ziel dieses Artikels ist die Aufklärung der Beziehung zwischen psychophysikalischer Lateralisation und den neuronalen Generatoren der korrespondierenden akustisch evozierten Potenziale. Es werden Vielkanal-EEG-Messungen früher akustisch evozierter Potenziale von 12 Versuchspersonen auf binaurale Klick-Stimuli mit verschiedenen interauralen Zeit- und Pegeldifferenzen analysiert. Die Daten werden durch äquivalente Stromdipole, die die generierenden Quellen im Gehirn repräsentieren, modelliert. Zur Lösung des inversen Problems wird eine verallgemeinerte Maximum-Likelihood-Methode unter Einbeziehung der Rauschkovarianzmatrix der Daten benutzt. Die Fitqualität wird durch den sog. goodness-of-fit als Ergebnis eines χ^2-Tests bestimmt. Dieses Maß ist gegenüber der konventionell verwendeten Restvarianz vorteilhaft. Zur Latenz von Jewett Welle V wurde eine systematische Variation des Moments eines rotierenden Dipols mit der Lateralisation des Stimulus gefunden. Dipolmomenttrajektorien für Stimuli mit ähnlicher Lateralisation sind ähnlich. Ein Vorzeichenwechsel der interauralen Parameter resultiert in einer Spiegelung der Trajektorie. Zentral wahrgenommene Stimuli entsprechen Dipolen mit den größten vertikalen Komponenten. Mit zunehmender Lateralisation nimmt die vertikale Momentkomponente ab, während die horizontale Komponente zunimmt. Die Ähnlichkeit zwischen den Trajektorien, die durch Stimuli mit gleicher Lateralisation hervorgerufen werden, zeigt, dass interaurale Zeit- und Pegeldifferenzen nicht unabhängig voneinander verarbeitet werden. Die Daten unterstützen die Hypothese, dass Richtungsinformation bereits auf der Ebene des Hirnstamms extrahiert und repräsentiert wird.

Schlüsselwörter: FAEP, Lateralisation, ITD, ILD, Dipolquellenanalyse

1 Introduction

Hearing with two ears allows to accurately localize sounds in space. The perceived spatial position of an acoustic stimulus predominantly depends on its interaural time difference (ITD) and its interaural level difference (ILD) [6, 11, 12, 22, 34, 35, 47, 62, 63]. In order not to blur the interaural information, the binaural system compares the inputs from both ears at a relatively early stage in the neural pathway. The first intersection of left and right auditory nerve fibers occurs at the superior olive (SO) within the brain stem [38]. Binaurally sensitive cells also reside in the subsequent brain stem nuclei, i.e., the lateral lemniscus (NLL) and the inferior colliculus (IC) [4, 5, 15, 16, 18, 19, 33, 58, 60, 61].

Evoked potentials have been widely used to investigate directional hearing in humans. The majority of the studies dealing with the dependence of auditory brain stem responses (ABRs) on ITD and ILD focused on the analysis of the waveforms of single EEG channels [2, 3, 7, 13, 14, 20, 24, 26, 28, 29, 32, 50, 59]. The so-called three-channel Lissajous' trajectory represents an attempt to infer the activity of the brain stem from ABR recordings. It is measured using three bipolar pairs of electrodes with preferably perpendicular orientation. The three time signals are then visualized as a trajectory in the three-dimensional voltage space [23, 42, 43]. Three-channel Lissajous' trajectories have been used to analyze binaural processing [39, 40, 41, 44, 45]. The benefit of the method is that it avoids the problem of the reference electrode by using a bipolar montage. However, it relies on the assumption of a single dipole located exactly in the center of the head, and volume conduction effects are not taken into account.

A more sophisticated approach to localize active neural tissue in the brain is dipole source analysis from multi-channel EEG measurements [27, 36, 52, 53, 54]. Scherg and von Cramon [55] proposed a model of six fixed current dipoles to describe the five waves of the monaurally evoked ABR. This model not only used a fixed location and orientation for each dipole, but also heavily constrained the time course of the dipole moment magnitude. The active structures at the latency of the largest deflection, wave V, were identifed as the superior olive and the lateral lemniscus.

The present study focuses on the source analysis of monaurally and binaurally evoked ABRs. In order to analyze the influence of lateralization, nine different binaural stimulus conditions, the combinations of three ITDs and three ILDs are used. Since the same lateralization can be generated by different combinations of the interaural differences, the variation of both cues allows to draw conclusions about the representation of the stimulus laterality in the brain stem.

2 Methods

2.1 Subjects

Twelve subjects (three females) from the staff of the University of Oldenburg without any history of audiological or neurological problems participated voluntarily in this study. They were aged between 25 and 36 years and were classifed as normal hearing by routine audiometry. The audiometric loss was less than 10 dB for frequencies below 4 kHz and less than 15 dB for the higher frequencies.

2.2 Stimuli

Rarefaction click stimuli were produced by applying rectangular voltage pulses of 100 µs duration to Etymotic Research ER-2 insert earphones. The time interval between the onsets of two successive stimuli was chosen to vary randomly and equally distributed between 62 and 72 ms, yielding an average stimulation rate of approximately 15 Hz.

15 stimulus conditions were tested, 9 binaural and 6 monaural. The monaural clicks were presented at the levels 53, 59 and 65 dB nHL and are denoted as L–m, L0m, L+m and R–m, R0m, R+m for monaural left and right stimulation, respectively. The binaural stimuli were the nine possible combinations of 3 ITDs (–0.4, 0 and 0.4 ms) and 3 ILDs (–12, 0 and 12 dB), as indicated in Figure 1.

The binaural stimuli are named as follows: the first letter refers to the perceived lateralization of the stimuli: 'L' for left,

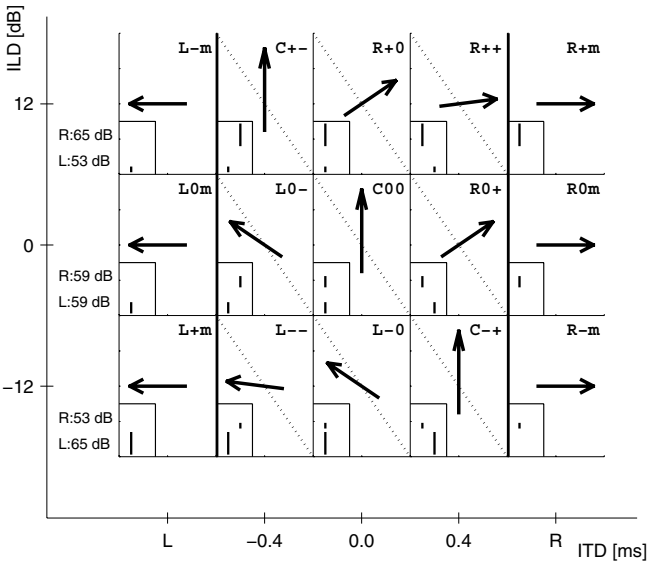

Figure 1 Naming convention and lateralization of the stimuli: centrally perceived stimuli are marked with a 'C'. Stimuli lateralized to the left and right side are marked with 'L' and 'R', respectively. For the monaural stimuli the second character indicates the level. For the binaural stimuli the second and third character denote the sign of ILD and ITD, respectively. Arrows point into the approximate direction of perceived lateralization. The insets in the lower left corner of each subplot schematically depict the time courses of left and right clicks, respectively. Time is on the horizontal axis, amplitude on the vertical axis. The dotted lines connect stimuli eliciting similar lateralization.

'C' for center and 'R' for right. The second and third characters ('–', '0' and '+') are used to specify the ILD and ITD, respectively. For example, for diotic stimulation, to both ears a click at 59 dB nHL was presented simultaneously. This stimulus C00 is found in the center of the diagram (ILD = ITD = 0). The stimulus R+0 in the middle of the top row has zero ITD, but is lateralized to the right due to its positive ILD. On the other hand, the stimulus R0+ at the right of the middle row has zero ILD, but is also lateralized to the right due to its positive ITD. The arrows in Figure 1 point into the approximate direction of the lateralization of the stimuli. Both an ITD of 0.4 ms and an ILD of 12 dB cause a strong, but not extreme lateralization of about 70° [13, 32]. A stronger, almost complete lateralization is produced by the synergistic stimuli L–– and R++ whose ILDs and ITDs point into the same direction. In contrast, the stimuli C+– and C–+ refer to the antagonistic situation: ILD and ITD act in opposite directions resulting in a centered image. In the lower left corner of each subplot in Figure 1, the respective binaural stimulus is depicted schematically. In the ITD-ILD-plane lines of equal lateralizaton are the diagonal dotted lines. Identical stimuli were used for all subjects for better comparability of the results.

2.3 Electrode configuration and recordings

Ag/AgCl-electrodes were attached to a fiexible cap worn by the subjects. ABRs were recorded from 32 sites according to the extended 10-20-system [21, 57] using a DC-coupled differential amplifier (Synamps 5803) at a samplingrate of 10 kHz with 16 bit resolution. The common reference electrode was placed at the vertex (Cz), the ground electrode at the forehead (Fpz). Electrode impedances were measured at a test signal frequency of 30 Hz and brought below 5 kΩ. 10000 single sweeps for all of the 15 stimuli were recorded in an interleaved manner. The electrode positions in the three-dimensional space were determined using a measuring instrument exploiting different ultrasonic signal propagation delays at different sensors (CMS30P by Zebris Medizintechnik). Details of the recording procedure can be found elsewhere [48, 50]. Before averaging, the single sweeps were filtered with a linear phase FIR bandpass with 200 taps and corner frequencies of 100 and 1500 Hz [17]. An iterated weighted average of the filtered sweeps was computed for all subjects and stimulus conditions [49].

2.4 Dipole source analysis

To fit a current dipole to the data, a software package was written in MATLAB. The head was modeled by a homogeneous sphere characterized by a constant volume conductivity $g = 0.0033\,\Omega^{-1}cm^{-1}$ [8]. The radius of the sphere was determined by fitting the electrode positions $\vec{r}_c$, $c = 1 \ldots C$, to a sphere in a least squares sense for each subject. The source was described by a single rotating dipole, i. e., its location $\vec{r}$ was fitted, but constrained to be constant for the time interval under consideration. For each time sample the three moment parameters $\vec{m}$ were adjusted. A rotating dipole has $P = 3 + 3T$ parameters, $N = 3$ nonlinear location parameters and $L = 3T$ linear moment parameter with T being the number of samples in the time interval. The forward model is given by the $C \times L$ leadfield matrix $\mathbf{F}(g, \vec{r}, \vec{r}_c)$ describing the modeled EEG of a unit dipole at location $\vec{r}$ measured at electrode positions $\vec{r}_c$. The modeled potentials were calculated by $\mathbf{V}_{\text{model}} = \mathbf{F}\vec{m}$.

The measured data was supposed to be contaminated with additive multivariate Gaussian noise [25]. The elements of the time-averaged noise covariance matrix $\mathbf{S}$ were estimated from the J single sweeps of a measurement according to

$$\sigma_{cd} = \frac{1}{T}\sum_{t=1}^{T}\frac{1}{J(J-1)}\sum_{j=1}^{J}\left(V_{cj}(t)-\mu_c(t)\right)\left(V_{dj}(t)-\mu_d(t)\right) \quad (1)$$

with c and d being the indices of two channels. $\mu_c(t) = 1/J\sum_{j=1}^{J}V_{cj}(t)$ represents the ensemble average, i. e., the evoked potential of channel c at time t. To minimize the difference between measured and modeled data, i. e., the residual $\mathbf{e} = \mathbf{V} - \mathbf{V}_{\text{model}}$, the cost function of generalized maximum-likelihood estimation

$$E_S = \mathbf{e}^T\mathbf{S}^{-1}\mathbf{e} = \sum_{c=1}^{C}\sum_{d=1}^{C} e_c\left[\mathbf{S}^{-1}\right]_{cd} e_d \quad (2)$$

was used. The resulting forward model that minimizes the cost function is termed 'the fit' $\mathbf{V}_{\text{fit}}$. In contrast, in the majority of EEG studies no noise information is utilized, i. e., $\mathbf{S} = \mathbf{1}$ is assumed, and solely the least squares error $E_1 = \mathbf{e}^T\,\mathbf{e} = \Sigma_{c=1}^{C}e_c^2$ is minimized. The search of the optimal dipole location $\vec{r}$ was performed by means of the simplex algorithm by Nelder and Mead [37]. Within the nonlinear fitting routine, the vector of the optimal moment parameters was directly determined by

$$\vec{\mathrm{m}} = (\mathbf{F}^T\mathbf{S}^{-1}\mathbf{F})^{-1}\,\mathbf{F}^T\mathbf{S}^{-1}\mathbf{V}. \quad (3)$$

2.4.1 Estimation of the parameter uncertainties

The $L \times L$ covariance matrix $\mathbf{S}_L$ of the linear moment parameters was determined by error propagation

$$\mathbf{S}_L = (\mathbf{F}^T\mathbf{S}^{-1}\mathbf{F})^{-1}. \quad (4)$$

The variances of the linear parameters are found on the diagonal of $\mathbf{S}_L$.

The $N \times N$ covariance matrix $\mathbf{S}_N$ of the nonlinear location parameters were estimated by calculating the curvatures in a small region around the minimum.

$$\mathbf{S}_N = \left(\vec{\nabla}_{\vec{r}}\,\mathbf{V}_{\text{fit}}^T\mathbf{S}^{-1}\,\vec{\nabla}_{\vec{r}}\,\mathbf{V}_{\text{fit}}\right)^{-1}. \quad (5)$$

$\vec{\nabla}_{\vec{r}}\mathbf{V}_{\text{fit}}$ is the $C \times N$ matrix of the partial derivatives of the forward model with respect to the nonlinear parameters.

2.4.2 Evaluation of the goodness-of-fit

The fit quality was assessed by the comparison of the residual $\mathbf{e}$, i. e., the difference between data and forward model, with

the noise in the measurement. If the residual is below or in the range of the measurement errors, the fit can be regarded as of good quality. On the other hand, if the deviation between model and data drastically exceeds the noise, the fit cannot be considered as satisfactory. In mathematical terms, the fit quality is assessed by means of a chi-square test. If only the noise variances are known, i. e., $\sigma_{cd} = \sigma_c^2 \delta_{cd}$, the cost function reduces to the one of ordinary maximum likelihood estimation

$$E_V = \sum_{c=1}^{C} (e_c / \sigma_c)^2 . \tag{6}$$

Under the assumption of Gaussian measurement errors the quantity e_c/σ_c is normally distributed with mean zero and variance one. Consequently, the cost function E_V is a sum of squared standard normal distributions and is therefore χ^2-distributed.

In the present work, the complete noise covariance matrix **S** resulting in the more general cost function E_S (eq. (2)) was used. However, E_S remains invariant under a unitary transform **U**, i. e., $\mathbf{U}^{-1} = \mathbf{U}^T$, into the eigen-system of $\mathbf{S}^{-1}$. With $\widehat{\mathbf{S}^{-1}} = \mathbf{U}\mathbf{S}^{-1}\mathbf{U}^T$ and $\widehat{\mathbf{e}} = \mathbf{U}\mathbf{e}$ it follows

$$\widehat{E_S} = \widehat{\mathbf{e}}^T \, \widehat{\mathbf{S}^{-1}} \, \widehat{\mathbf{e}} = \mathbf{e}^T \mathbf{U}^T \mathbf{U} \, \mathbf{S}^{-1} \, \mathbf{U}^T \mathbf{U} \, \mathbf{e} = \mathbf{e}^T \mathbf{S}^{-1} \, \mathbf{e} = E_S . \tag{7}$$

Since $\widehat{\mathbf{S}^{-1}}$ is diagonal, $\widehat{E_S}$ has the form of E_V (eq. (6)). As a consequence, E_S also obeys a χ^2-distribution. E_S^*, denoting E_S at the end of the fitting procedure, is distributed as a χ^2-distribution with $\nu = C - P$ degrees of freedom [46]. The goodness-of-fit (gof) was calculated using the incomplete gamma function Γ_{inc}:

$$\text{gof} = 1 - \Gamma_{\text{inc}} \left(\frac{E_S^*}{2}, \frac{\nu}{2} \right) = 1 - \frac{\int_0^{E_S^*/2} x^{\frac{\nu}{2}-1} \, \mathrm{e}^{-x} \, dx}{\int_0^{\infty} x^{\frac{\nu}{2}-1} \, \mathrm{e}^{-x} \, dx} . \tag{8}$$

The goodness-of-fit is the area under the χ^2-density function with ν/2 degrees of freedom integrated from half the minimal error $E_S^*/2$ to infinity. It is interpreted as the probability that the residual **e**, i. e., the difference between model and data, can be considered as measurement noise. For vanishing error E_S^* gof approaches 1. For increasing E_S^* the numerator approaches the denominator resulting in a decreasing gof. The χ^2-distribution has a mean of ν and a variance of 2ν. Therefore, gof-values above 0.1 are considered as good, above 0.001 as acceptable, models with gof < 0.001 should be rejected [46]. The goodness-of-fit is determined by the ratio of E_S^* and ν. For $C = 32$ channels and a single time instant a dipole has $\nu = 26$ degrees of freedom. If for each channel the deviation between model and data equals the standard error of that channel, E_S^* amounts to 32 and gof to 0.193 which is rated as a good fit.

For the purpose of comparison, the so-called residual variance, which is widely used in the literature, was also computed

$$\text{rv} = \frac{\sum_{c=1}^{C} (V_{\text{fit},c} - V_c)^2}{\sum_{c=1}^{C} V_c^2} = \frac{E_1}{P_{\text{global}}} \tag{9}$$

The residual variance rv is the least-squares cost function normalized by the global power of the measured signal P_{global}. Therefore it should be termed 'normalized residual variance', however, we follow the expression 'residual variance' prevailing in literature.

A detailed description of the source analysis strategy used in the present study can be found in [48].

3 Results

Figure 2 shows ABRs of one subject for all 32 measured channels in recording reference. For each channel three responses are depicted: the response to the diotic stimulus (C00) in the top trace, the monaural left response (L0m) in the middle trace, and the monaural right response (R0m) in the bottom trace. The residual noise for each channel and condition is shown by the error bars. They denote the threefold standard error of the mean (±3 S.E.M.). Channels near the reference electrode (Cz) generally exhibit smaller responses and smaller residual noise compared to channels more distant from Cz. Exceptions are channels Fp2 and F4 which show irregular waveforms. However, these channels also have large standard errors. While a least squares fit would incorporate these irregular waveforms into the dipole fit, the maximum likelihood method is not distracted by these irregularities because it takes into account the raised residual noise in these channels.

In Figure 3 the locations of a rotating dipole for all stimulus conditions and subject DJ are shown. Data were fitted for a time interval from 1 ms before to 1 ms after the latency of wave V. This 2-ms interval comprises 21 samples and will be used in the subsequent analysis. Note that its beginning and end depend on stimulus condition and subject. The optimized locations are inferior to the center of the head, about 2.7 cm below the horizontal plane. The fitted locations from the binaural conditions (filled symbols) form a narrow cluster. Their 95 %-confidence regions (ellipses) at t_V have a diameter of about 0.4 cm. The locations of the monaural left and right conditions are found 0.5 cm to the right and left from the midline (x = 0), respectively. The 95 %-confidence regions of the monaural conditions (open symbols) have roughly twice the size of those from the binaural conditions (0.8 cm). For subject DJ the spatial separation of the dipoles fitted to the monaural stimuli is most pronounced across subjects, it amounts to approximately 1 cm. In the average over subjects, the mean distance in x-direction between dipoles corresponding to monaural left and right stimuli is only 0.4 cm.

Figure 4 shows the dipole moment trajectories of the rotating dipole fitted in the interval from 1 ms before to 1 ms after peak V in the frontal plane. Data are averaged over subjects. The triangle denotes the start of the trajectory at $t_V - 1$ ms. The ellipses drawn at t_V are the 95 %-confidence regions for the dipole moment. They do not vary over time because neither the leadfield matrix **F** nor the covariance

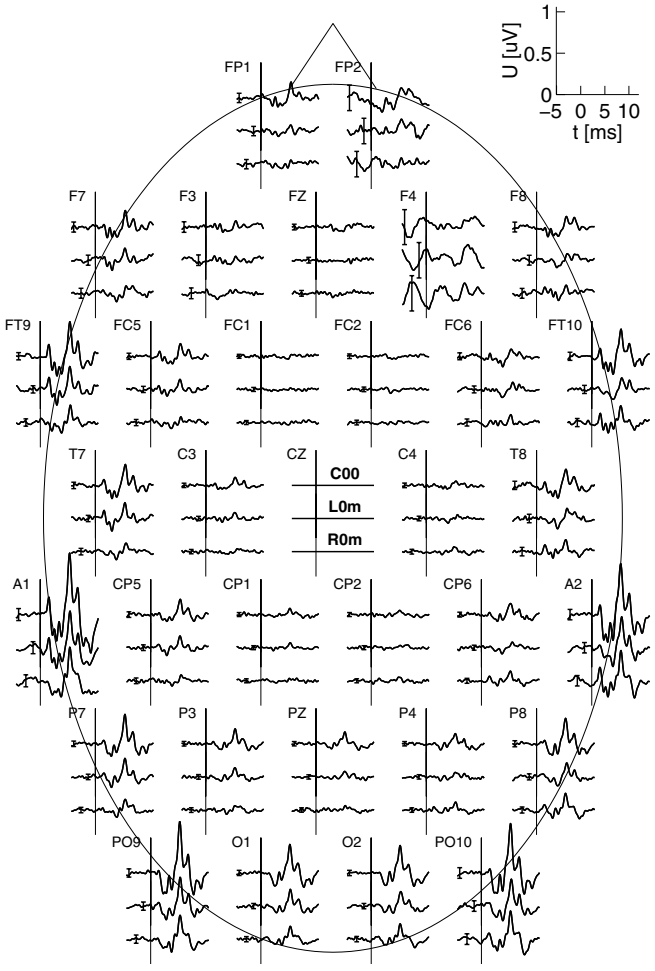

Figure 2 ABRs recorded from 32 channels for subject JO. Data are plotted in recording reference, the reference electrode was Cz. Top trace: binaural response to the diotic click (C00). Middle trace: response to monaural left click (L0m). Bottom trace: response to monaural right click (R0m). The error bars indicate ±3 standard errors of the mean.

matrix **S** are time dependent (cf. eq. (4)). The trajectories for the central stimuli, i. e., the diotic stimulus C00 and the antagonistic stimuli (C+– and C–+), exhibit the largest dipole moments in the vertical direction (m_z). With growing lateralization, m_z decreases and is smallest for the monaural conditions. The moment trajectories allow to distinguish between left and right conditions. For stimuli which are lateralized to the right clockwise trajectories are observed while counter-clockwise trajectories are found for left-lateralized stimuli. Furthermore, for the conditions with ITD only and ILD only the trajectories look very similar. The trajectories to R+0 and R0+ as well as to L–0 and L0– bear a strong resemblance to each other. This is striking since they are produced by different physical stimuli but elicit the same subjective lateralization.

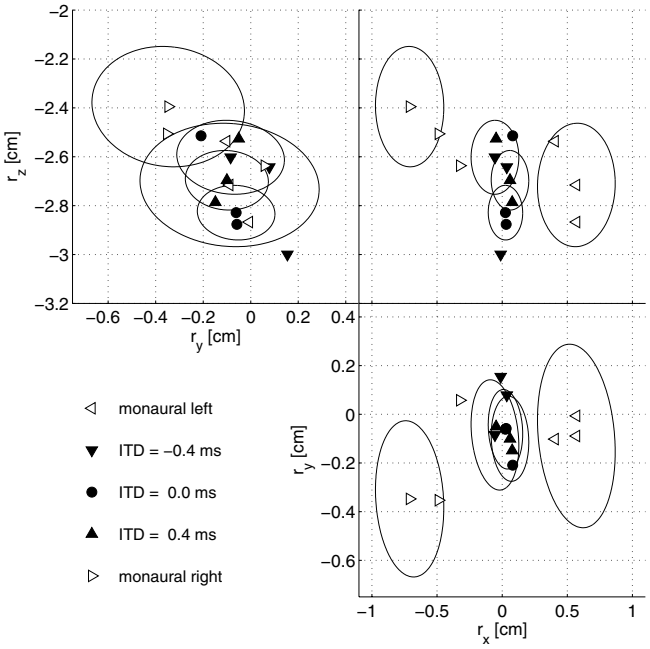

Figure 3 Locations of rotating dipoles fitted to the 15 conditions for subject DJ. x points to the right, y to the front and z to the top. The fit interval began 1 ms before and ended 1 ms after the latency of wave V (t_V). Filled symbols denote binaural stimuli, open symbols stand for monaural stimuli. The 95%-confidence regions (ellipses) hold for t_V, they are only drawn for the three binaural stimuli with ILD = 0 dB and the two monaural stimuli with intermediate level.

Figure 5 shows the characteristics of signal and noise, and exemplifies the two measures of fit quality applied. Data are ABRs from diotic stimulation of subject HR. In the upper left panel (A), the rms-value of the signal averaged over the 32 measurement channels, i. e., $\sqrt{P_{\text{global}}}$ is shown. Wave V at a latency of 5.8 ms is the most pronounced peak of the ABR, its rms-value is 248 nV. The straight line in Figure 5B at 9.3 nV is the rms-value of the noise level averaged over channels, i. e., the square root of the global noise power. Since the noise fluctuations over time are small they were averaged over time [49]. The noise level varies very little between stimulus conditions, but considerably between subjects (rms-values are in the range from 8.9 to 16.5 nV, mean 11.8 nV). The residual **e** is the difference between measured EEG **V** and forward model $\mathbf{V}_{\text{fit}}$. Its rms-value averaged over channels is also plotted in Figure 5B. It varies substantially over time, at t_V it is maximal and amounts to 17.3 nV. Whereas for illustration only the average over channels is depicted in the upper panels of Figure 5, the fitting routine uses noise and residual individually for each channel, cf. eq. (2). In Figure 5C, the residual variance rv (eq. (9)) is shown. It is mainly determined by its denominator: at small signal energies, rv is found to be large and vice versa. As a consequence, despite the maximal residual at t_V of 17.3 nV, rv amounts to only 0.005 or half a percent. On the other hand,

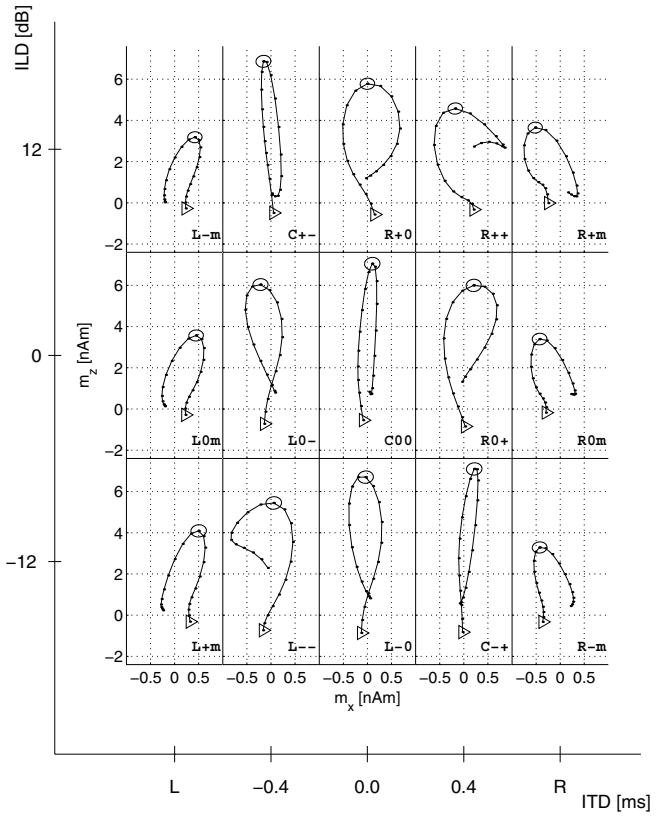

Figure 4 Dipole moment trajectories of a rotating dipole for the 15 stimulus conditions in the frontal plane, mean over subjects. The x-coordinate points to the right, z to the top. The fit interval lasted 2 ms, from 1 ms before (triangles) to 1 ms after peak V. At the latency of wave V, ellipses denoting the 95 %-confidence regions for the dipole moment are drawn.

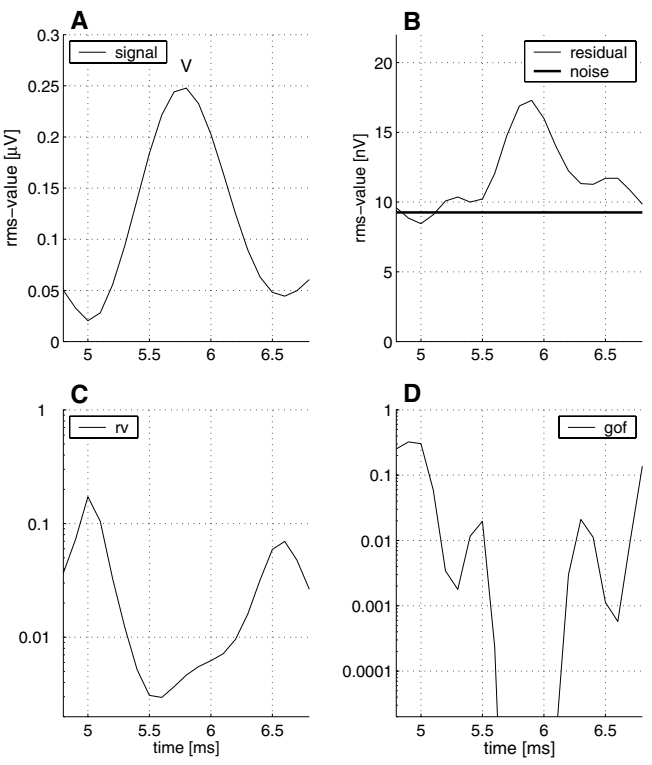

Figure 5 Signal characteristics and measures of the fit quality for the rotating dipole fit. Data from subject HR, response to the diotic click. A: signal rms. B: rms of the difference between signal and fit (residual, thin line) compared to the residual noise averaged over time and channels (straight thick line). C: residual variance (rv). D: goodness-of-fit (gof).

Figure 5D depicts the goodness-of-fit (gof, eq. (8)) as the outcome of the χ^2-test. At time instants where the residual is smaller than the noise, gof is near 1. At t_V gof is very low since the residual is nearly twice the noise, i. e., it is very unlikely that the deviation between data and model is due to the noise. Although at t_V 99.5 % of the variance of the data is explained by the model, the fit cannot not be regarded as good because of the low gof. However, a reduction of the number of sweeps from 10000 to 2500 would approximately double the residual noise and generate gof-values near one. The residual noise would be virtually unaffected by such a change of the noise level.

Figure 6 shows the quality measures of the rotating dipole fit for the mean over subjects and all stimulus conditions. At t_V the residual variance (thin lines) is about 2 % for the monaural (and synergistic) stimuli and roughly 1 % for the binaural stimuli. The monaural responses have approximately half the amplitude of the binaural responses and therefore exhibit roughly twice the rv. The goodness-of-fit values (thick lines) are high for the monaural stimuli and markedly lower for the binaural stimuli implying that the monaurally evoked potentials are well described by a single dipole while the binaurally evoked potentials are not. This finding cannot be inferred from the residual variance.

4 Discussion

The aim of this work is to analyze the correspondence between psychophysical lateralization and the neural generators of potentials evoked by lateralized stimuli. Since the generators of early auditory evoked potentials are deep, i. e., reside in the brain stem, data exhibit a relatively low SNR (signal-to-noise ratio). Therefore a large number of sweeps per stimulus condition (10000) was collected to ameliorate the signal quality.

4.1 Incorporation of the noise covariance matrix

To enhance and accurately determine the quality of the solutions of the inverse problem, information of the measurement

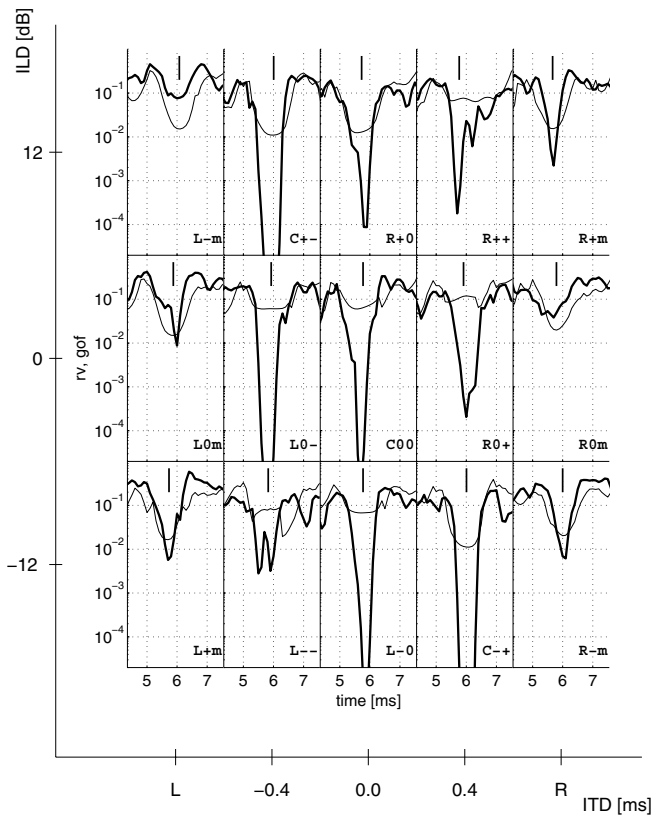

Figure 6 Residual variance (rv, thin lines) and goodness-of-fit (gof, thick lines) of the rotating dipole fit for all stimulus conditions, mean over subjects. The vertical bars mark the mean latency of wave V.

errors based on the single sweeps of the EEG recordings was used [49]. The noise covariance matrix allows (i) a more general formulation of the cost function, (ii) the computation of confidence regions for source parameters by error propagation, and (iii) the evaluation of the fit quality by means of a statistical test. Generalized maximum likelihood estimation was first used by Sekihara et al. [56] who analyzed the biomagnetic inverse problem. Lütkenhöner [30, 31] demonstrated the advantage of the incorporation of noise covariance both theoretically and with MEG (magnetoencephalogram) data from late auditory evoked potentials. The current paper extends these findings to auditory brain stem responses that exhibit a markedly lower SNR.

4.2 Goodness-of-fit versus residual variance

An important methodological improvement pertains to the judgement of fit quality. In EEG literature the residual variance rv is commonly used to determine the quality of the fit. It has two major drawbacks. First, it introduces a kind of 'quadratic bias'. A residual variance of 1 % sounds reasonably small, but is equivalent to a residual standard deviation of 10 %. Second, the rv does not compare the residual with the noise in the measurement. Therefore it should be considered as not being appropiate for rating the fit quality. Without noise information it is also impossible to infer confidence regions of source parameters.

The goodness-of-fit (gof) allows to decide if it is necessary to improve the source model in order to better explain the data. The single dipole model is sufficient for the monaural conditions. Since the gof unveiled significant differences between data and model for the binaural conditions, it is reasonable to analyze a more complex model, e. g., a model using two dipoles, one for a brain stem nucleus in each hemisphere [48]. Such conclusions can not be drawn from the analysis of the residual variance which indicates a better fit quality for the binaural conditions. In commercial software programs like BESA (Brain Electrical Source Analysis) and ASA (Advanced Source Analysis) noise information is not considered, i. e., **S** is set to the unit matrix. The fit quality is expressed in terms of rv. Given the sophisticated algorithms which are used in data analysis, e. g., distributed source models or the computation of forward models using realistically shaped head models, it is surprising that the judgement of noise and SNR of data has such a low significance.

4.3 The rotating dipole

Despite the small extension of the brain stem, significantly different dipole locations were detected for monaural and binaural stimuli. For binaural stimuli a centered source with a 95 %-confidence region radius as small as 2 mm is found for subjects with high SNR. For monaural stimuli the fitted dipole position is found in the contralateral hemisphere. This is physiologically meaningful because the majority of the auditory fibers projects to contralateral nuclei in the brain stem [38]. However, the distance between left and right fitted source amounts to maximally 1 cm. Given the anatomical distance of the likely generators of wave V, namely 1.6 cm for the superior olives and 2.2 cm for the nuclei of the lateral lemniscii, the fitted distances appear as being too small.

Two reasons are conceivable to explain this discrepancy. First, the homogeneous sphere which served as head model may be too simple because it does not model the attenuation effect of the skull. Compared to the brain tissue and the skin, the conductivity of the skull is about 80 times smaller [8]. Ary et al. [1] compared the homogeneous sphere with a three-shell head model. They showed that a dipole in the 3-shell head model must have a larger excentricity to generate approximately the same EEG as an identically oriented dipole in a homogeneous sphere. Second, for monaural stimulation the ipsilateral generators will also be activated, albeit weaker. The fitting algorithm has to optimize a single source that must explain two sources of different strengths. It consequently finds the best matching position between both sources which is located nearer to the stronger source.

Additionally, the rotating dipole fit unveils characteristics of the generators. Centrally perceived stimuli cause trajectories of the dipole moment in the frontal plane that mainly extend in the

vertical direction. Lateral stimuli generate trajectories with smaller vertical but larger horizontal extension. This corresponds well to the results from [50], taking into account that the single channels A1, A2, PO9 and P010 are orientated predominantly vertical and therefore map the vertical component m_z of the source dipole. The laterality of the stimulus is coded in the sense of rotation of the trajectory. The moment trajectories of the rotating dipole do not code the ITD or ILD alone, but show a striking correlation with the lateralization of the stimuli (see Figs. 1 and 4), i. e., stimuli with similar lateralization cause similar dipole moment trajectories. This means that ITD and ILD are not processed independently in the brain stem.

4.4 Possible improvements

A three-shell model of the head can be used instead of the homogeneous sphere. It is generally believed that by means of realistically shaped head models derived from MRI (magnetic resonance imaging) scans, the localization accuracy can be augmented. However, recently Cuffin et al. [9] compared the source localization errors of the three-shell model with a realistically shaped head model. The sources were created by injecting current into implanted depth electrodes of human patients. Virtually no difference occurred in the localization errors of both models.

Alternatively, the number of recording channels can be raised to improve spatial sampling. Residual noise can be further reduced by even longer recording sessions. Presumably, evoked potentials to only a few stimulus conditions can be collected. Instead of the click a rising frequency chirp [10, 51] generating larger evoked potentials with a higher SNR is a promising alternative.

5 Summary and conclusions

- The incorporation of the noise covariance matrix into the algorithm to solve the inverse problem allows to derive confidence regions for dipole parameters and to apply a statistical test to evaluate the fit quality.
- The goodness-of-fit, comparing the residual with the noise, is preferable to the residual variance which relies only on the residual and does not account for the noise in the recording.
- Rotating dipoles corresponding to binaural stimuli are localized in the sagittal plane.
- For monaural stimuli, the locations of the rotating dipoles lie in the hemisphere contralateral to the side of stimulation.
- The moments of the rotating dipoles strongly correlate with the lateralization of the stimuli caused by ITD *and* ILD, but they do not correlate with ITD or ILD alone.

Acknowledgements

The present work was supported by the *Deutsche Forschungsgemeinschaft* through the *Sonderforschungsbereich Neurokognition* (SFB 517).

References

[1] Ary, J. P., Klein, S. A., Fender, D. H.: Location of sources of evoked scalp potentials: corrections for skull and scalp thicknesses. IEEE Trans. Biomed. Eng. **28(6)** (1981) 447–452

[2] Brantberg, K., Fransson, P. A., Hansson, H., Rosenhall, U.: Measures of the binaural interaction component in human auditory brainstem response using objective detection criteria. Scand. Audiol. **28(1)** (1999) 15–26

[3] Brantberg, K., Hansson, H., Fransson, P. A., Rosenhall, U.: The binaural interaction component in human ABR is stable within the 0- to 1-ms range of interaural time differences. Audiol. Neurootol. **4** (1999) 88–94

[4] Caird, D., Klinke, R.: Representation of sound frequency and laterality by units in the central nucleus of cat inferior colliculus. Exp. Brain. Res. **52** (1983) 385–399

[5] Caird, D., Sontheimer, D., Klinke, R.: Intra- and extracranially recorded auditory evoked potentials in the cat: I. Source location and binaural interaction. Electroenceph. clin. Neurophysiol. **61** (1985) 50–60

[6] Colburn, H. S., Durlach, N. I.: Models of binaural interaction. In: E. C. Carterette, M. P. Friedman (Eds.): Handbook of Perception – Hearing. Academic Press, New York, vol. IV, chap. 11. pp. 467–518 (1978)

[7] Cone-Wesson, B., Ma, E., Fowler, C. G.: Effect of stimulus level and frequency on ABR and MLR binaural interaction in human neonates. Hear. Res. **106** (1997) 163–178

[8] Cuffin, B. N., Cohen, D.: Comparison of the magnetoencephalogram and electroencephalogram. Electroenceph. clin. Neurophysiol. **47(2)** (1979) 132–146

[9] Cuffin, B. N., Schomer, D. L., Ives, J. R., Blume, H.: Experimental tests of EEG source localization accuracy in spherical head models. Clin. Neurophysiol. **112** (2001) 46–51

[10] Dau, T., Wegner, O., Mellert, V., Kollmeier, B.: Auditory brain stem responses with optimized chirp signals compensating basilar-membrane dispersion. J. Acoust. Soc. Am. **107(3)** (2000) 1530–1540

[11] Durlach, N. I., Colburn, H. S.: Binaural phenomena. In: E. C. Carterette, M. P. Friedman (Eds.): Handbook of Perception – Hearing. Academic Press, New York, vol. IV, chap. 10. pp. 365–466 (1978)

[12] Feddersen, W. E., Sandel, T. T., Teas, D. C., Jeffress, L. A.: Localization of high-frequency tones. J. Acoust. Soc. Am. **29** (1957) 988–991

[13] Furst, M., Levine, R. A., McGaffigan, P. M.: Click lateralization is related to the β component of the dichotic brainstem auditory evoked potentials of human subjects. J. Acoust. Soc. Am. **78(5)** (1985) 1644–1651

[14] Gerull, G., Mrowinski, D.: Brain stem potentials evoked by binaural click stimuli with differences in interaural time and intensity. Audiology **23** (1984) 265–276

[15] Goldberg, J. M., Brown, P. B.: Functional organization of the dog superior olivary complex: an anatomical and electrophysiological study. J. Neurophysiol. **31** (1968) 639–656

[16] Goldberg, J. M., Brown, P. B.: Response of binaural neurons of dog superior olivary complex to dichotic tonal stimuli: some physiological mechanisms of sound localization. J. Neurophysiol. **36** (1969) 157–178

[17] Granzow, M., Riedel, H., Kollmeier, B.: Single-sweep-based methods to improve the quality of auditory brain stem responses. Part I: Optimized linear filtering. Z. Audiol. **40(1)** (2001) 32–44

[18] Gummer, A. W., Zenner, H.-P.: Central processing of the auditory information. In: R. Greger, U. Windhorst (Eds.): Comprehensive Human Physiology, Springer, Berlin, vol. 1, chap. 36. pp. 729–756 (1996)

[19] Irvine, D. R.: Physiology of the auditory brainstem. In: A. N. Popper, R. R. Fay (Eds.): The Mammalian Auditory Pathway: Neurophysiology. Springer, New York, vol. 2, chap. 4. pp. 153–231 (1992)

[20] Ito, S., Hoke, M., Pantev, C., Lütkenhöner, B.: Binaural interaction in brainstem auditory evoked potentials elicited by frequency-specific stimuli. Hear. Res. **35** (1988) 9–20

[21] Jasper, H. H.: The ten twenty electrode system of the international federation. Electroenceph. clin. Neurophysiol. **10** (1957) 371–375, appendix

[22] Jeffress, L. A., McFadden, D.: Differences of interaural phase and level in detection and lateralization. J. Acoust. Soc. Am. **49(4)** (1971) 1169–1179

[23] Jewett, D. L.: The 3-channel Lissajous' trajectory of the auditory brainstem response. IX. Theoretical aspects. Electroenceph. clin. Neurophysiol. **68** (1987) 386–408

[24] Jiang, Z. D.: Binaural interaction and the effects of stimulus intensity and repetition rate in human auditory brain-stem. Electroenceph. clin. Neurophysiol. **100** (1996) 505–516
[25] John, E. R., Harmony, T., Valdes-Sosa, P.: The use of statistics in electrophysiology. In: A. S. Gevins, A. Rémond (Eds.): Handbook of Electroencephalography and Clinical Neurophysiology. Elsevier, Amsterdam, vol. 1, chap. 16. pp. 497–540 (1987)
[26] Jones, S. J., van der Poel, J. C.: Binaural interaction in the brain-stem auditory evoked potential: evidence for a delay line coincidence detection mechanism. Electroenceph. clin. Neurophysiol. **77** (1990) 214–224
[27] Kavanagh, R. N., Darcey, T. M., Lehmann, D., Fender, D. H.: Evaluation of methods for threedimensional localization of electrical sources in the human brain. IEEE Trans. Biomed. Eng. **25(5)** (1978) 421–429
[28] Levine, R. A.: Binaural interaction in brainstem potentials of human subjects. Ann. Neurol. **9** (1981) 384–393
[29] Levine, R. A., Davis, P. J.: Origin of the click-evoked binaural interaction potential, β, of humans. Hear. Res. **57(1)** (1991) 121–128
[30] Lütkenhöner, B.: Dipole source localization by means of maximum likelihood estimation I. Theory and simulations. Electroenceph. clin. Neurophysiol. **106(4)** (1998) 314–321
[31] Lütkenhöner, B.: Dipole source localization by means of maximum likelihood estimation. II. Experimental evaluation. Electroenceph. clin. Neurophysiol. **106(4)** (1998) 322–329
[32] McPherson, D. L., Starr, A.: Auditory time-intensity cues in the binaural interaction component of the auditory evoked potentials. Hear. Res. **89** (1995) 162–171
[33] Melcher, J. R., Kiang, N. Y. S.: Generators of the brain-stem auditory-evoked potential in cat. 3. Identified cell-populations. Hear. Res. **93(1–2)** (1996) 52–71
[34] Mills, A. W.: On the minimum audible angle. J. Acoust. Soc. Am. **30** (1958) 237–246
[35] Mills, A. W.: Lateralization of high-frequency tones. J. Acoust. Soc. Am. **32** (1960) 132–134
[36] Mosher, J. C., Lewis, P. S., Leahy, R. M.: Multiple dipole modeling and localization from spatiotemporal MEG data. IEEE Trans. Biomed. Eng. **39(6)** (1992) 541–557
[37] Nelder, J. A., Mead, R.: A simplex method for function minimization. The Computer Journal **8** (1965) 308–313
[38] Nieuwenhuys, R., Vogel, J., van Huijzen, C.: The Human Central Nervous System – a Synopsis and Atlas. Springer, Berlin (1988)
[39] Polyakov, A., Pratt, H.: Three-channel Lissajous' trajectory of the binaural interaction components in human auditory brain-stem evoked potentials. Electroenceph. clin. Neurophysiol. **92** (1994) 396–404
[40] Polyakov, A., Pratt, H.: Evidence for spatio-topic organization of binaural processing in the human brainstem. Hear. Res. **94** (1996) 107–115
[41] Polyakov, A., Pratt, H.: The effect of binaural masking noise disparity on human auditory brainstem binaural interaction components. Audiology **37** (1998) 17–26
[42] Pratt, H., Har'el, Z., Golos, E.: Three-channel lissajous' trajectory of human auditory brain stem evoked potentials. Electroenceph. clin. Neurophysiol. **56** (1983) 682–688
[43] Pratt, H., Martin, W. H., Kaminer, M., Bleich, N.: Three-channel lissajous' trajectories of auditory brain stem evoked potentials. Quantitative measures, effects of stimulus parameters and clinical promise. In: F. Grandori, M. Hoke, G. L. Romani (Eds.): Auditory Evoked Magnetic Fields and Electric Potentials. Karger, Basel, vol. 6, pp. 331–356 (1990)
[44] Pratt, H., Polyakov, A., Aharonson, V., Korczyn, A. D., Tadmor, R., Fullerton, B. C., Levine, R. A., Furst, M.: Effects of localized pontine lesions on auditory brain-stem evoked potentials and binaural processing in humans. Electroenceph. clin. Neurophysiol. **108** (1998) 511–520
[45] Pratt, H., Polyakov, A., Kontorovich, L.: Evidence for separate processing in the human brainstem of interaural intensity and temporal disparities for sound lateralization. Hear. Res. **108** (1997) 1–8
[46] Press, W. H., Teukolsky, S. A., Vetterling, W. T., Flannery, B. P.: Numerical Recipes in C, the Art of Scientific Computing. Cambridge University Press, Cambridge (1992)
[47] Rayleigh, L. S. J. W.: On our perception of sound direction. Philos. Mag. **13** (1907) 214–232
[48] Riedel, H.: Analysis of early auditory evoked potentials elicited by stimuli with directional information. Ph.D. Thesis, University of Oldenburg, Germany, Oldenburg (2002)
[49] Riedel, H., Granzow, M., Kollmeier, B.: Single-sweep-based methods to improve the quality of auditory brain stem responses. Part II: Averaging methods. Z. Audiol. **40(2)** (2001) 62–85
[50] Riedel, H., Kollmeier, B.: Auditory brain stem responses evoked by lateralized clicks: Is lateralization extracted in the human brain stem ? Hear. Res. **163(1-2)** (2002) 12–26
[51] Riedel, H., Kollmeier, B.: Comparison of binaural auditory brain stem responses and the binaural difference potential evoked by chirps and clicks. Hear. Res. **169(1-2)** (2002) 85–96
[52] Scherg, M.: Spatio-temporal modelling of early auditory evoked potentials. Rev. Laryngol. Otol. Rhinol. **105(2, suppl.)** (1984) 163–170
[53] Scherg, M.: Fundamentals of dipole source potential analysis. In: F. Grandori, M. Hoke, G. L. Romani (Eds.): Auditory Evoked Magnetic Fields and Electric Potentials. Karger, Basel, vol. 6. pp. 40–69 (1990)
[54] Scherg, M.: Akustisch evozierte Potentiale: Grundlagen – Entstehungsmechanismen – Quellenmodell. Kohlhammer, Stuttgart (1991)
[55] Scherg, M., von Cramon, D.: A new interpretation of the generators of BAEP waves I-V: results of a spatio-temporal dipole model. Electroenceph. clin. Neurophysiol. **62** (1985) 290–299
[56] Sekihara, K., Ogura, Y., Hotta, M.: Maximum-likelihood estimation of current-dipole parameters for data obtained using multichannel magnetometer. IEEE Trans. Biomed. Eng. **39(6)** (1992) 558–562
[57] Sharbrough, F., Chatrian, G.-E., Lesser, R. P., Lüders, H., Nuwer, M., Picton, T. W.: American Electroencephalographic Society Guidelines for Standard Electrode Position Nomenclature. J. Clin. Neurophysiol. **8(2)** (1991) 200–202
[58] van Adel, B. A., Kidd, S. A., Kelly, J. B.: Contribution of the commissure of Probst to binaural evoked responses in the rat's inferior colliculus: interaural time differences. Hear. Res. **130** (1999) 115–130
[59] Wrege, K. S., Starr, A.: Binaural interaction in human auditory brainstem evoked potentials. Arch. Neurol. **38** (1981) 572–580
[60] Yin, T. C., Chan, J. C.: Neural mechanisms underlying interaural time sensitivity to tones and noise. In: G. M. Edelman, W. E. Gall, W. M. Cowan (Eds.): Auditory Function: Neurobiological Bases of Hearing. John Wiley and Sons, New York, chap. 13. pp. 385–430 (1988)
[61] Yin, T. C. T., Chan, J. C. K.: Interaural time sensitivity in medial superior olive of cat. J. Neurophysiol. **64(2)** (1990) 465–488
[62] Yost, W. A.: Lateral position of sinusoids presented with interaural intensive and temporal difference. J. Acoust. Soc. Am. **70(2)** (1981) 397–409
[63] Yost, W. A., Gourevitch, G.: Directional Hearing. Springer, New York (1987)

Received 24. 04. 2002; accepted for publication 21. 02. 2003.

Correspondence to:

Dr. Helmut Riedel
Medizinische Physik, Universität Oldenburg,
D-26111 Oldenburg
e-mail: helmut.riedel@uni-oldenburg.de